Robust μ Synthesis Control Design for a High Speed Integrated Motor/Compressor System Supported by AMBs

Long Di[a] and Zongli Lin[b]

[a] ASML-HMI, 1762 Automation Pkwy, San Jose, CA 95131, USA, ld4vv@virginia.edu
[b] Charles L. Brown Department of Electrical and Computer Engineering, and Rotating Machinery and Control Laboratory (ROMAC), University of Virginia, Charlottesville, VA 22904-4743, USA, zl5y@virginia.edu

***Abstract*—Active magnetic beatings (AMBs) have been gradually adopted in high-speed rotating machinery applications and the control design plays a critical role in AMB systems. The μ synthesis control is one of the most sophisticated robust control design methods and it considers both robust stability and performance. The resulting controller is able to handle uncertainties in the dynamic system and achieve required performance and stability margin, which makes it an ideal solution for AMB control problems. However, since μ synthesis control design directly depends on the dynamic model, an accurate modeling process of the AMB system needs to be performed prior to the controller design. In this research, we apply the robust μ synthesis control design to a high speed integrated motor/compressor system supported by AMBs. It briefly describes the modeling of the test rig, summarizes the μ synthesis control design process and presents the control simulation results. The simulation results have shown that the designed μ synthesis controller is able to achieve strong control performance as well as strong robustness for the analyzed AMB system.**

I. Introduction

High-speed rotating machineries supported by active magnetic bearings (AMBs) have found more and more applications in the industry [1]. As the rotating speed increases, the unbalance forces, the gyroscopic effect and the high frequency flexible modes all affect the operation of the machine. Since the controller plays a critical role in the operation of an AMB system, its design entails significant consideration. For a system with complex dynamics, such as a high speed integrated motor/compressor system supported by AMBs, a controller with simple structure might not be adequate to achieve the stability and performance requirements. Therefore, advanced controllers are introduced.

Most advanced controllers require system models, which can be difficult to obtain for practical AMB systems. Besides, the design process can be time consuming, especially when large modeling errors are present. The integrated motor/compressor system analyzed in this work is designed to operate beyond first bending, which indicates that a potentially large unbalance force can be introduced to induce instability to the AMB system. Meanwhile, the rising speed range is wider than typical machines so that the gyroscopic effect can split the natural modes more significantly, which will introduce strong uncertainties. Therefore, for the AMB system to be analyzed, a successful control design must both guarantee the closed-loop stability and minimize the vibration during the speed increase and at the operational speed. In order to satisfy the stringent performance specifications in the face of uncertainties, the μ-synthesis control design is adopted.

The μ-synthesis approach is able to better handle uncertainties in a complex system and achieve strong performance [2]. To obtain such result, it requires a relatively accurate characterization of the plant dynamics and uncertainties, which might be often difficult to derive. On the other hand, since we have accumulated much knowledge on the modeling of high speed rotating machineries, such a requirement has becomes much less stringent. When the synthesis is completed, this robust controller can effectively meet two design objectives, stability robustness and performance robustness. The first guarantees the closed-loop stability of the system in the presence of uncertainties. The latter ensures that not only all the possible uncertain systems remain stable, but also have acceptable closed-loop performance.

The μ-synthesis design aims to minimize the structure singular value μ of the open-loop interconnection of the nominal plant model, uncertain parameters, un-modeled system dynamics, and performance and uncertainty weighting functions. The weighting functions correspond to the specifications for the required performance [2], [6]. For AMB systems, weighting functions that have been considered include the vibration criteria and the magnetic force limit; the model uncertainties include the speed-dependent gyroscopic effect and the simulated cross-coupled stiffness using exciter AMBs.

This paper is organized as follows. First, the test rig is briefly introduced in Section 2. Then we describe the entire AMB system model and show the modeling results in Sections 3 and 4, respectively. Afterwards, in Sections 5 and 6, the robust μ-synthesis control design method is presented and verified by simulations. The concluding remarks are made in Section 7.

II. AMB System Model

The AMB system model for the integrated motor/compressor machine equipped with AMBs incorporates the rotor finite element (FE) model, the linearized AMB model, the sensor and amplifier models, and the Padé approximation model of the computational delay [3], [4]. The block diagram of the rotor AMB system is shown in Fig. 1.

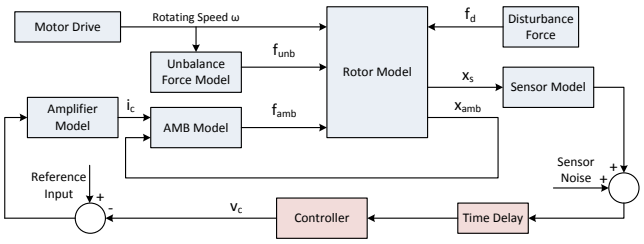

Figure 1: A block diagram of the AMB system .

A. Rotor Model

A two dimensional FE model of the rotor is obtained by dividing the length into 87 stations for the lateral rotor dynamic analysis. Each station of the rotor is modeled as a lumped mass-stiffness element while the discs and the AMB laminations are modeled as mass-inertia elements added to certain locations. A four degree of freedom (DOF) lateral analysis is performed for each node and it generates global entries for the mass (M), internal shaft stiffness (K), internal shaft damping (D) and gyroscopic (G) matrices. Matrices M, K and D are symmetric and positive definite while matrix G is skew-symmetric. The dynamic motion of the rotor can be described by the following second order equation,

$$M\ddot{q} + (D + \Omega G)\dot{q} + Kq = B_{mag}F_{mag} + B_w F_w,$$
$$y_r = Cq,$$

where the displacement vector q contains 348 elements representing the lateral translations in x and y axes, rotating angles about y and x axes, F_{mag} represents the forces provided by the AMBs and B_{mag} specifies the location where the forces are injected, F_w includes all external forces acting on the rotor with B_w specifying the locations, Ω is the rotational speed, and the vector y_r represents the rotor displacement at the sensor locations specified by the output matrix C. The modeling assumes that there is no axial motion of the rotor.

The critical speed analysis of the rotor as a function of the supporting bearing stiffness is shown Fig. 2. The closed-loop stiffness is targeted between 1e6 N/m and 1e7 N/m. To visualize the gyroscopic effect on splitting the system natural frequencies into forward and backward modes, a Campbell diagram is also generated in Fig. 3. When the running speed lines (1X) and (2X) intersect with the rotor natural frequencies, synchronous or super-synchronous vibrations are induced. These vibrations need to be well-contained with sufficient damping.

The mode shape plot is another important tool to analyze the rotordyanmic performance. Since all modes that can be excited should be observable and controllable, the AMBs and sensors should be placed at locations where motions with enough amplitude occur. In addition, the sensor locations need to be in phase with the AMB locations for each natural mode to avoid the non-collocation issue. Based on the damped mode shape plot of the rotor with modal damping at 0.2%, it has been verified that the non-collocation issue is minor.

Based on the coordinate transformation between the physical space and the modal space using $q = \Phi_m \zeta$, the rotor

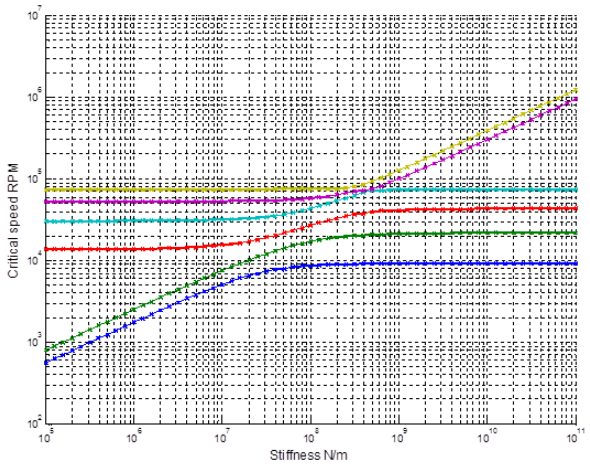

Figure 2: The critical speed map of the rotor.

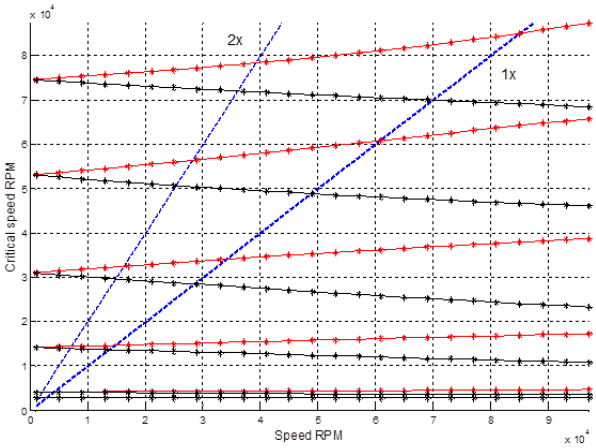

Figure 3: The Campbell diagram of the rotor.

state space model can be converted into the following modally reduced state space form

$$\begin{bmatrix}\dot{\zeta}_x(t)\\ \dot{\zeta}_y(t)\end{bmatrix} = \begin{bmatrix}A_\zeta & \Omega G\\ -\Omega G & A_\zeta\end{bmatrix}\begin{bmatrix}\zeta_x(t)\\ \zeta_y(t)\end{bmatrix} + \begin{bmatrix}\Phi_m^{\mathrm{T}} B_{mag} & 0\\ 0 & \Phi_m^{\mathrm{T}} B_{mag}\end{bmatrix} F_{mag} + \begin{bmatrix}\Phi_m^{\mathrm{T}} B_w & 0\\ 0 & \Phi_m^{\mathrm{T}} B_w\end{bmatrix} F_w,$$
$$y_r = \begin{bmatrix}C_x\Phi_m & 0\\ 0 & C_x\Phi_m\end{bmatrix}\begin{bmatrix}\zeta_x(t)\\ \zeta_y(t)\end{bmatrix}.$$

The original state space model has 696 states and contains several high order rotor modes beyond the controller bandwidth. These modes are unlikely to be excited and contribute negligible effect to the system dynamics. Thus, in order to facilitate designs and analysis, model truncation is applied to obtain reduced order model. The final rotor model retains the

two rigid body modes and the first four bending modes with a total of 24 states and is represented as follows,

$$\begin{aligned} \dot{x}_m &= A_m x_m + B_m F_{mag} + B_d F_w, \\ y_r &= C_m x_m. \end{aligned}$$

B. Modeling of AMB

The forces generated by AMBs depend on the air gap between the rotor and the stator, as well as the current feedings in the windings on the stator. The net force generated by the pair of AMBs can be described as

$$F_{mag} = k_x x + k_i i_c, \tag{1}$$

where x is the rotor displacement at the AMB location, i_c is the control current, k_x is the open loop stiffness, and k_i is the open loop current gain of the AMB.

This AMB model ignores the eddy current loss and assumes zero leakage in the magnetic circuit. Combining the rotor model with the linearized AMB model, we arrive at the following system model

$$\begin{aligned} \dot{x}_m &= \Big(A_m - B_m k_x [B_{mag} \quad 0]\Big) x_m + B_m k_i i_c + B_d F_w, \\ &= \hat{A}_m x_m + B_m k_i i + B_d F_w, \\ y_r &= C_m x_m. \end{aligned}$$

C. The Entire AMB System

Based on the fitting with the experimental frequency response, the power amplifier is modeled by a third order transfer function as follows,

$$G_a(s) = \frac{d_a}{(s+p_a)(s^2 + 2\xi_1\omega_1 s + \omega_1^2)} \text{ A/V}, \tag{2}$$

where d_a is the amplifier dc gain.

The amplifier transfer function $G_a(s)$ is then converted into a state space model (A_a, B_a, C_a) with a total of 12 states for all the control channels.

The eddy current type displacement sensor is modeled by the following transfer function

$$G_s(s) = \frac{d_s}{(s+p_s)}, \tag{3}$$

where d_s is the current sensor gain.

The sensor transfer function $G_s(s)$ is converted into a state space model (A_s, B_s, C_s) with 4 states.

To model the computational delay caused by the DSP, a second order Padé approximation is used to obtain a rational transfer function for an approximated time delay as follows

$$e^{-\tau s} = \frac{e^{-\frac{1}{2}\tau s}}{e^{\frac{1}{2}\tau s}} \tag{4}$$

$$\approx \frac{1 - \frac{1}{2}\tau s + \left(\frac{1}{2}\tau s\right)^2}{1 + \frac{1}{2}\tau s + \left(\frac{1}{2}\tau s\right)^2}. \tag{5}$$

The Padé approximation can be formulated into a state space model (A_f, B_f, C_f) that contributes 8 additional states. The final system model incorporating the rotor, AMBs, amplifiers, sensors and time delay can be described in the following form, with 76 states, 6 inputs and 4 outputs.

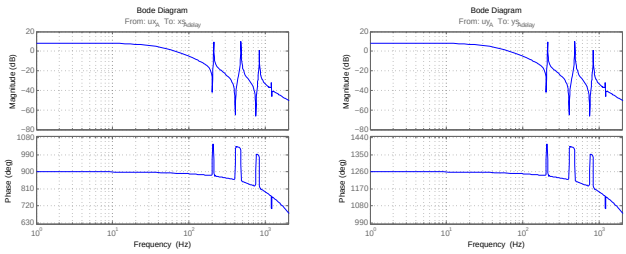

(a) Radial bearing x axis. (b) Radial bearing y axis.

Figure 4: Radial bearing open loop transfer functions.

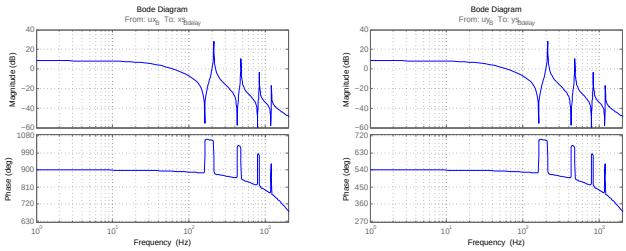

(a) Combo radial x axis. (b) Combo radial y axis.

Figure 5: Combo radial open loop transfer functions.

$$\begin{bmatrix} \dot{x}_m \\ \dot{x}_s \\ \dot{x}_a \\ \dot{x}_f \end{bmatrix} = \begin{bmatrix} \hat{A}_m & 0 & B_m k_i C_a & 0 \\ B_s C_m & A_s & 0 & 0 \\ 0 & 0 & A_a & 0 \\ 0 & B_f C_s & 0 & A_f \end{bmatrix} \begin{bmatrix} x_m \\ x_s \\ x_a \\ x_f \end{bmatrix} + \begin{bmatrix} 0 \\ 0 \\ B_a \\ 0 \end{bmatrix} u + \begin{bmatrix} B_d \\ 0 \\ 0 \\ 0 \end{bmatrix} F_w,$$

$$y_f = C_f x_f.$$

III. Modeling Results

After tweaking the rotor model, the first 6 resonances are included in the current system model. The bodeplot in Figs. 4 and 5 also show that the radial bearing and the combo radial bearing sides have different transfer functions (TFs). It can be verified that the non-collocation issue is minor based on the bode plots of the radial bearing as the zero/pole locations are switched for the fourth bending mode, which is much less influential than the other bending modes. The rotor models considering the eigenmode uncertainties are also shown in Figs. 6 and 7, where the rotor resonant frequencies change $\pm 5\%$ and the corresponding uncertain state-space (USS) system models are utilized for the μ-synthesis control design.

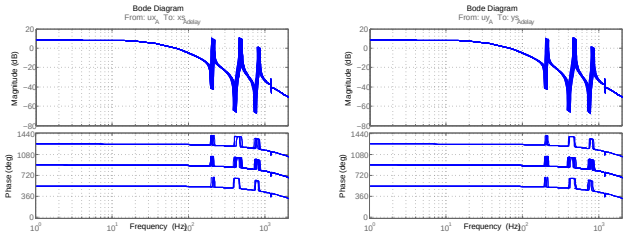

(a) Radial bearing x axis. (b) Radial bearing y axis.

Figure 6: Rotor transfer functions considering the model uncertainties (Radial bearing).

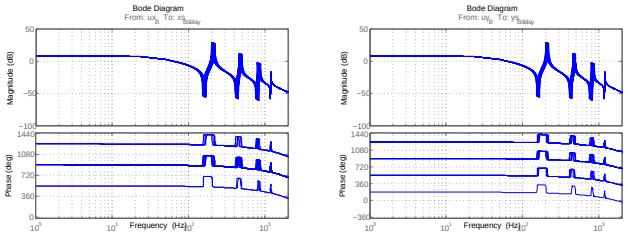

(a) Combo radial x axis. (b) Combo radial y axis.

Figure 7: Rotor transfer functions considering the model uncertainties (Combo radial bearing).

IV. μ-Synthesis Control

The μ-synthesis control studied in this project is the only multivariable control design we have come up that guarantees performance specification while considering both plant uncertainties and external perturbations [2]. This section first describes the tools for the synthesis process and the uncertainty models for AMB systems, and then it details the selection of the weighting function and shows the final synthesized controller. In addition, the μ-analysis is also included.

A. Tools for Synthesis

Shown in Fig. 8 is the interconnection among the plant G, the controller K and the uncertainty block Δ. In the figure, u is the control signal and y is the measured output, w is the external disturbance signal, z is the output performance signal, and Δy and v are the input and output signals associated with the uncertainty block.

The closed-loop stability analysis includes both robust stability and robust performance analysis. To ensure that the closed-loop system remains robustly stable in consideration of all modeling uncertainties, the H_∞ optimization is typically applied to the robust controller design [5]. In addition, to ensure that the design performance objectives are satisfied for all possible plant under the uncertainty set, the μ-analysis is used in the evaluation of the resulting closed-loop system.

For the H_∞ optimization problem, it aims to find a feedback controller that minimizes the H_∞ norm of the closed-loop system considering the external disturbance as input [5]. Meanwhile, several design requirements are included that are imposed through weighting functions. Assuming that the internal stability of the nominal system is achieved through the

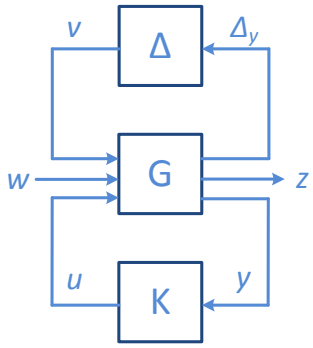

Figure 8: $\Delta - G - K$ feedback connection used during synthesis.

H_∞ controller, the μ-synthesis expands the capability of the controller to not only minimize the H_∞ norm of the nominal system, but also all systems under the uncertainty set such that

$$\min_K \left\| F_u\big(F_l(G,K),\Delta\big)\right\|_\infty, \tag{6}$$

and the robust performance is satisfied if and only if

$$\mu_\Delta\big(F_l(G,K)\big) < 1, \tag{7}$$

where F_l defines the connection between G and K and F_u defines the connection between F_l and Δ.

For $\Delta(s)$ to be stable, it satisfies $\left\|\Delta(s)\right\|_\infty < 1$, and μ_Δ is the structured singular value defined as

$$\mu_\Delta\big(F_l(G,K)\big) := \frac{1}{\min\{\bar{\sigma}(\Delta) : \Delta \in \mathbf{\Delta}, \det(I - N\Delta) = 0\}}, \tag{8}$$

where $N := F_l(G,K)$ that defines the feedback connection between $G(s)$ and the controller $K(s)$.

The μ-synthesis approach does not have a unique global solution based on the general form. Therefore, it typically introduces a stable and minimum phase scaling matrix D that satisfies $D\Delta = \Delta D$, and then μ_Δ can be approximated by the upper bound as

$$\mu_\Delta(N) :\leq \inf_{D\in D} \bar{\sigma}\big(DF_l(G,K)D^{-1}\big), \tag{9}$$

which can be considered as an upper bound on the linear fractional transformation of the generalized plant G regarding the controller K.

Afterwards, the μ-synthesis design can be formulated as finding a controller K that achieves

$$\min_K \inf_D \left\| DND^{-1}\right\|_\infty. \tag{10}$$

The controller is typically designed through $D-K$ iteration, which iterates the design process until the upper bound on the structured singular value of the closed-loop system is below 1. The standard $D-K$ iteration is summarized as follows,

1) By first fixing the D scale ($D = I$), finding an H_∞ controller K that minimizes $\left\|DND^{-1}\right\|_\infty$. When $\left\|DND^{-1}\right\|_\infty < 1$ or no longer decreases, the iteration stops and the controller K achieving the lowest norm is adopted for the design.

2) With the fixed controller K, finding a stable minimum-phase scale D that minimizes the maximum structured singular value $\bar{\sigma}\big(DND^{-1}(jw)\big)$.
3) With the updated D, the controller synthesis iterates until the robust performance requirement is achieved such that

$$\mu_{\Delta}(N) \leq \min_{D \in D} \bar{\sigma}\big(DND^{-1}\big) < 1. \tag{11}$$

The derived μ-synthesis controller has the same order as the sum of the order of the plant, the weighting functions and twice the order of the D scale. To achieve practical final controller, model reduction is typically applied. In addition, these steps are not all convex so the global optimum might not exist or convergence might not be achieved when the plant model has high order or the plant, uncertainty models, weighting functions have poor numerical conditioning.

B. Uncertainty Models

Plant parameter deviations lead to potential degradation of the system stability and performance. For an AMB system, which is open-loop unstable and time varying, the uncertainties need to be scrutinized in more detail. The primary uncertainty is due to the un-modeled system dynamics, such as the modal damping, which is typically assumed to be $\pm 10\%$. The rotational speed dependent gyroscopic effects or load-dependent cross-coupled stiffness effects can drive the system modes away from the nominal locations, which is typically assumed to be $\pm 5\%$ of the resonant frequencies.

To better characterize the uncertainty models, the nominal plant model should be derived by proximity to the average values of the critical parameters. The uncertainty models can then be generated based on the nominal plant by varying certain parameters. In order to maximize the performance of the closed-loop system, characterizing a concise uncertainty model is quite important but also challenging. The model uncertainty can be either structured or unstructured, where structured uncertainties are typically related to known parameters in the model, such as mass and stiffness, while unstructured uncertainties are related to the un-modeled or poorly modeled system dynamics, such as high frequency resonance. To add unstructured uncertainty effect, typical approach is to include the frequency dependent perturbation $\Delta(s)$ to a nominal system $G_n(s)$, such as $G_n(s) + \Delta(s)$ or $G_n(s)(1 + \Delta(s))$.

One of the most significant uncertainties in a rotor AMB system is the gyroscopic effect and it couples the dynamics of the x and y axes. According to the state space model derived for the AMB system, the system matrix is affected by the rotational speed, which indicates that the natural frequencies of the rotor might vary. For lightly damped bending modes, they might easily get excited with higher rotational speeds as the unbalance disturbance force gets larger. Based on the Campbell diagram shown in Fig. 3, the gyroscopic effect drives each rotor mode to split into forward and backward components and such uncertainty can be modeled as follows:

1) Defining the rotational speed Ω as an uncertain parameter varying from 0 rpm to max speed.
2) Defining the rotor eigenvalues affected by the gyroscopic effect with uncertain natural frequencies.
3) Defining the rotor mode damping as an uncertain parameter varying from 1% to 5%.

C. Weighting Function Selection

For time domain analysis, the percentage overshoot and the settling time are typical performance specifications. For an AMB system, since the transient response is generally not analyzed and the unbalance response at different rotational speed is the most critical, the frequency domain analysis becomes the primary approach to quantify the performance specification of AMB systems.

To analyze AMB system in the frequency domain, the sensitivity function is commonly used. For the plant G and the controller K, if we consider the plant output y and the reference input r, the external disturbance forces d_i and d_o on the plant input and output, the sensor noise n and the controller output u, the following sensitivity functions can be defined:

- Input sensitivity function $S_i = 1/(1 + KG)$: a measure of disturbance rejection at plant inputs;
- Output sensitivity function $S_o = 1/(1+GK)$: a measure of noise rejection and the closed-loop command tracking performance;
- Complementary input sensitivity function $T_i = KG/(1+GK)$: a measure of the effect of the disturbance at the reference input on the control output;
- Complementary output sensitivity function $T_o = GK/(1 + KG)$: a measure of the effect of the noise on the control output;
- Process sensitivity function $S_p = G/(1+KG)$: a measure of the closed-loop mechanical compliance of the rotor-bearing system;
- Control sensitivity function $S_c = K/(1+GK)$: a measure of the control output.

To meet the required performance specification, the sensitivity functions need to comply with certain bounds and it takes the following form for the output sensitivity function

$$\big\|W_s(s)S_o(s)\big\|_{\infty} < 1, \tag{12}$$

where $W_s(s)$ is the weighting function as well as a stable and proper transfer function.

Once the norm is satisfied, the inverse weighting W_s^{-1} represents the upper bound of the sensitivity function. For a MIMO AMB system, single sensitivity function is not sufficient to accommodate all the performance requirements at different degrees of freedom. Therefore, to satisfy the disturbance rejection requirement as well as the control bandwidth and reference tracking requirements simultaneously, several weighted sensitivity functions have to be considered at the same time. For example, $\big\|W_d(s)S_o(s)\big\|_{\infty} < 1$, $\big\|W_u(s)S_c(s)\big\|_{\infty} < 1$, $\big\|W_r(s)T(s)\big\|_{\infty} < 1$, $\big\|W_p(s)S_p(s)\big\|_{\infty} < 1$, and they can be

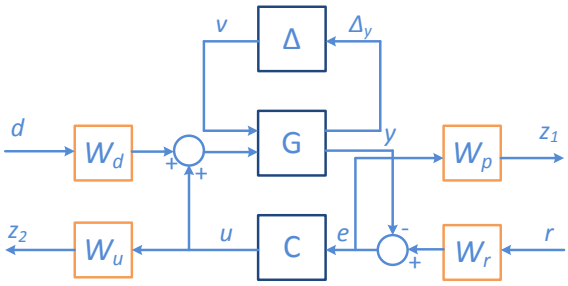

Figure 9: Feedback connection of the weighting functions to the plant, the uncertainty block and the controller.

grouped into one objective function as follows,

$$\min_{K} \left\| \begin{matrix} W_d(s)S_o(s) \\ W_u(s)S_c(s) \\ W_r(s)T(s) \\ W_p(s)S_p(s) \end{matrix} \right\| < \gamma, \tag{13}$$

where the maximum performance satisfying all the criteria after making trade-off can be achieved using the H_∞ synthesis process.

Fig. 9 illustrates the interconnection of the performance weight functions with the plant, the uncertainty block and the controller. Both the reference input r and the disturbance input d are considered as the external disturbance signals while the feedback error e and the control output u are two important indicating signals of the system performance.

The control sensitivity function S_c should be shaped such that the control output roll-off at high frequencies to avoid excitation of the un-modeled dynamics or sensor noise. The process sensitivity function S_p and the output sensitivity function S_o are typically shaped to achieve sufficient damping for certain modes and to enhance the disturbance rejection property. Based on Fig. 9, the following relation can be established between the performance signals z_1 and z_2 and the disturbance signal d and the reference input r,

$$\begin{bmatrix} z_1 \\ z_2 \end{bmatrix} = T_{zw} \begin{bmatrix} d \\ r \end{bmatrix}, \tag{14}$$

and in order to guarantee that the desired performance can be achieved, the cost γ to be minimized by the synthesized control K must be less than unity, which results in

$$\min_{K} \left\| T_{zw} \right\|_\infty < \gamma, \tag{15}$$

$$\left\| \begin{bmatrix} W_p(I+GK)^{-1}W_r & W_pG(I+GK)^{-1}W_d \\ W_uK(I+GK)^{-1}W_r & W_uGK(I+GK)^{-1}W_d \end{bmatrix} \right\|_\infty < \gamma. \tag{16}$$

Therefore, $(W_pW_r)^{-1}$, $(W_pW_d)^{-1}$, $(W_uW_r)^{-1}$ and $(W_uW_d)^{-1}$ are the upper bounds for S, GS, KS and T, respectively, and solving the cost function above solves the nominal performance problem. To solve the robust performance problem, the structured uncertainty set $\mathbf{\Delta}$ is defined and the $D-K$ iteration described in the previous section is applied to synthesize such a controller that minimizes $\mu_\Delta(N)$.

To satisfy the norm requirement as specified above, choosing suitable weighting functions become critical. The frequency dependent weighting functions are formulated in the following form

$$W_r(s) = K_1 \frac{s+\omega_1}{s+\omega_2}, \tag{17}$$

while the remaining static weighting functions simply take the scalar gains as follows,

$$W_p(s) = \frac{1}{M_1}, \quad W_u(s) = \frac{1}{M_2}, \quad W_d(s) = \frac{1}{M_3}. \tag{18}$$

As the performance requirements of the four channels in the studied AMB system are similar, the same weighting functions are used for each channel with diagonal weighting function matrix as follows,

$$W_r(s) = \text{blkdiag}\left\{W_{r,rx}, W_{r,ry}, W_{r,cx}, W_{r,cy}\right\}, \tag{19}$$

$$W_p(s) = \text{blkdiag}\left\{W_{p,rx}, W_{p,ry}, W_{p,cx}, W_{p,cy}\right\}, \tag{20}$$

$$W_u(s) = \text{blkdiag}\left\{W_{u,rx}, W_{u,ry}, W_{u,cx}, W_{u,cy}\right\}, \tag{21}$$

$$W_d(s) = \text{blkdiag}\left\{W_{d,rx}, W_{d,ry}, W_{d,cx}, W_{d,cy}\right\}, \tag{22}$$

where rx, ry, cx and cy correspond to the x and y axes of the radial bearing side and the combo radial bearing side, respectively. To further improve the performance, the scalars for each channel can be also adjusted separately.

D. The Synthesized Controller

Five different μ-synthesis controllers have been synthesized using a combination of different weighting functions. The $D-K$ iteration procedure is able to converge after 5 iterations to generate a stabilizing controller of order 80. The following table summarizes the $D-K$ iteration result for the final controller. The closed-loop complex and mixed μ value of the controller is shown in Fig. 10.

Since $\mu_\Delta(N) < 1$, the controller is able to guarantee that the performance satisfies the performance spec or the uncertainty description or both at the same time. Since the reciprocal of the actual μ value specifies how much the performance spec and the uncertainty set can be scaled before the robust performance (RP) objective is not guaranteed, the value only indicates the relative performance. Therefore, it is important to identify how much the stability, the performance and the uncertainty contribute to the total μ value.

Iteration	1	2	3	4	5
Controller Order	80	80	80	80	80
Total D-Scale Order	0	0	0	0	0
γ Achieved	315.125	0.583	0.509	0.509	0.509
Peak μ Value	300.59	0.514	0.498	0.498	0.498

The current size of the final control has 80 states prior to discretization. If the computing resource is more constrained, the size can be further reduced by using the Hankel norm

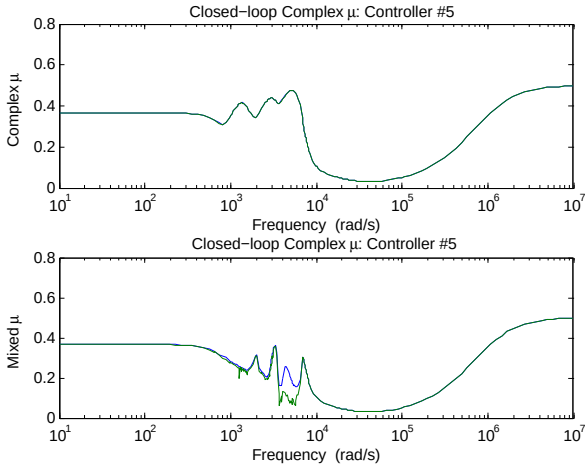

Figure 10: Closed-loop complex and mixed μ values of the synthesized controller.

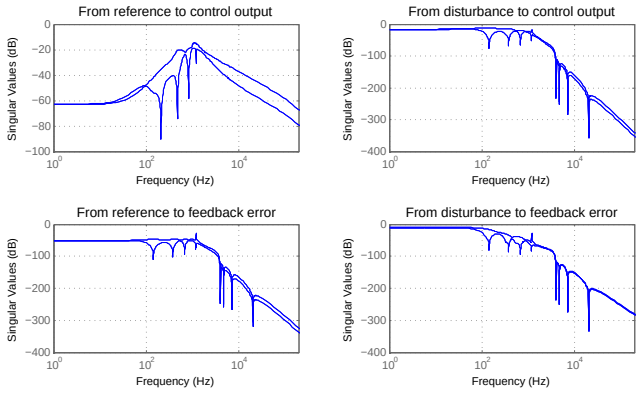

Figure 11: Singular value plot of the closed-loop inteconnected system.

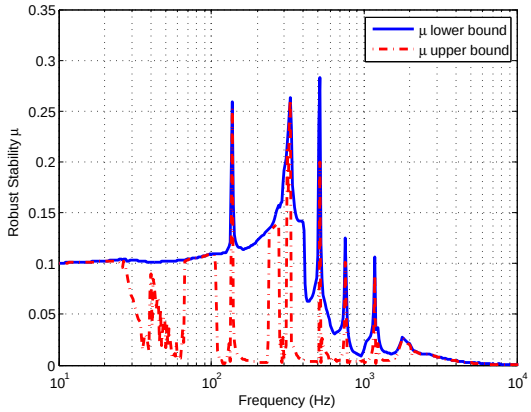

Figure 12: The robust stability bounds.

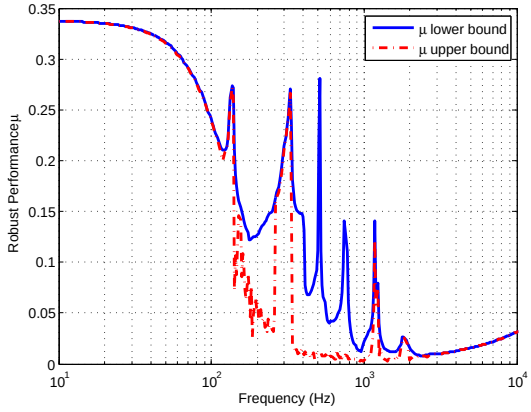

Figure 13: The robust performance bounds.

approximation. The analysis of the controller is mainly focused on the Bode plots and the singular value plots, where the controlled magnitude and phase response are analyzed. Shown in Fig. 10 is the closed-loop complex and mixed μ value of the synthesized controller and it is observed that the final peak is around 0.5.

Based on the synthesized controller, the singular value plot of the closed-loop interconnected system is shown in Fig. 11. The singular value plot illustrates the weighted input and output sensitivity functions from the reference input to the control output and feedback error locations, and from the disturbance input to the control input and feedback error locations.

E. The μ Analysis

When the peak μ value $\mu_\Delta(M) \leq 1$, $\forall\omega$, it can be easily concluded that the synthesized K satisfies the performance specification when the worst case perturbation is injected in the uncertainty block Δ. However, analysis also needs to be performed when the peak μ value does not satisfy the requirement to determine whether the performance specification is too tight or the uncertainty set is out of a reasonable range.

The robust stability is one of the major criteria for μ analysis. It computes an upper bound of the generalized structured singular value of the plant and controller with respect to the block-diagonal uncertainty structure described in the previous section.

The robust stability margin is essentially the reciprocal of the structured singular value. Therefore, upper bounds of the structured singular value become lower bounds on the stability margin. Then the destabilizing frequency where the μ upper bound peaks or where the stability margin is smallest can be identified. As shown in Fig. 12, it is observed that the lower bound is around 3.53 while the upper bound is 3.94, and the critical frequency is at 135.9 Hz.

The robust performance is another main criterion for μ analysis. Similar to the robust stability margin, the robust performance margin is also calculated based the reciprocal of the structured singular value. As shown in Fig. 13, it is observed that the lower bound and upper bound are both 2.96 at the low frequency range. The sensitivity functions with 20 random samples are also simulated when the rotational speed is 0 rpm. The maximum and minimum singular values are shown in Fig. 14, which indicate that the robustness requirements are satisfied.

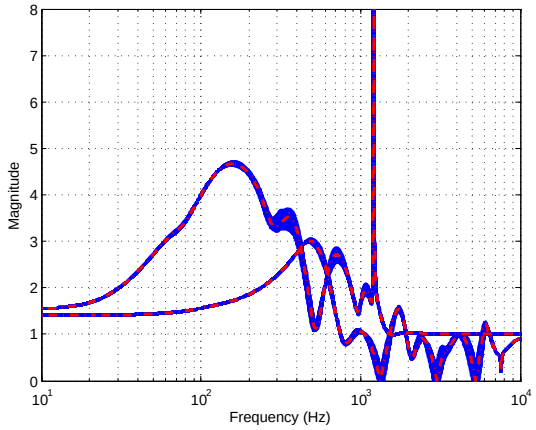

Figure 14: Sensitivity functions with 20 random samples.

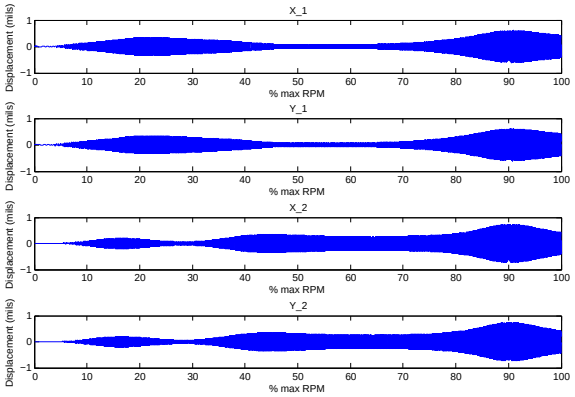

Figure 15: The rotor displacements of the four radial axes in mm from 0 rpm to max speed.

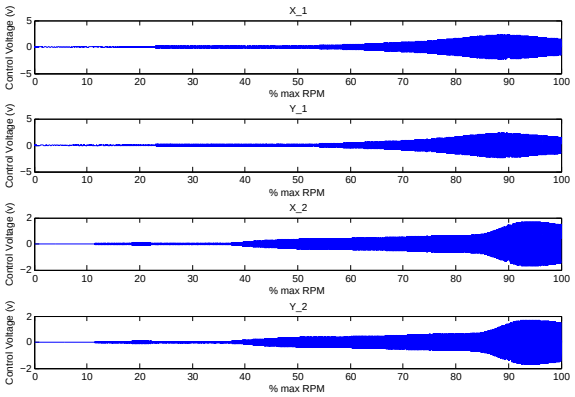

Figure 16: The control voltages of the four radial axes from 0 rpm to max speed.

F. The Rotordynamic Analysis

After a suitable μ-synthesis controller is designed and applied to the AMB system, the damped rotordynamic analysis can be performed to provide a more practical assessment of the rotor behavior and a typical approach is to analyze the forced unbalance response. The forced response subject to unbalance can be used to predict the actual performance of the AMB system over the designed operational speed range and API 617 has provided the most relevant standard for the analysis.

To conduct such analysis, the vibration level of the rotor over its operational speed range under certain imbalance conditions is collected and the imbalance is emulated by applying known masses to different locations along the rotor. While the rotational speed increases, the residual unbalance force excites the rotor resonances and the vibration amplitude at different speeds must comply with the guidelines. Based on the API guideline, the unit unbalance eccentricity u_b is

$$u_b = 27.4\ g \cdot mm. \tag{23}$$

To test the worst case scenario, the eccentricity is scaled by 4 and thus $4u_b$ is placed at the disk location to excite the rotor resonances. During the simulation, it is required that the unbalance response needs to remain within 30% of the radial clearance and the control perturbation current remains less than 80% of the bias over the entire rotational speed range. These standards directly come from our previous experience on μ-synthesis control design and they suggest the power bandwidth of the actuators still stay within the range even under the worst case situation.

V. Simulation Results

To verify the μ-synthesis controller method, numerical simulation on the AMB system model derived from the actual test rig has been carried out. The simulation program is constructed in Matlab Simulink and the main modeling block for the AMB system is formulated through the Matlab S-function, which makes the interface more compact and the program more flexible for additional changes on the test rig model.

In the simulation, the rotational speed increases from 0 to maximum design speed, which is also the designed operating speed range of the actual test rig. The rotor vibration at the four control axes are recorded with the increasing of the rotational speed to ensure that the vibration level never exceeds 30% of the radial clearance. Meanwhile, the control output is also displayed to verify that the control effort is within the amplifier saturation limit.

Shown in Fig. 15 is the rotor vibrations in mils for x and y axes of the motor and compressor side AMBs. It can be observed that the vibrations are well contained and are much smaller than the radial clearance. The small vibrations over a wide range of speeds demonstrate the effectiveness and robustness of the μ-synthesis controller. Shown in Fig. 16 is the control voltage for all the axes over the entire speed range. By confirming the limit of the actual amplifiers used on the test rig, it can be verified whether the current voltage output satisfies the actuator saturation requirement.

VI. Conclusions

In this paper, the robust μ synthesis control design is applied to a high speed integrated motor/compressor system supported by AMBs. A finite element model is first constructed for the integrated compressor system and based on the FEM model,

a state space model is derived for the MIMO μ-synthesis controller design. The μ-synthesis controller is designed by considering the model uncertainties and including proper weighting functions. Uncertainties with respect to resonance mode shifting and gyroscopic effect have been taken into consideration. The designed μ-synthesis controller is able to cover the full speed range with the unbalance response satisfying the radial clearance requirement. Simulation results have shown that the designed μ-synthesis controller is able to achieve strong control performance as well as strong robustness for the analyzed AMB system.

REFERENCES

[1] G. Schweitzer and E. H. Maslen, Magnetic Bearings. Berlin: Springer-Verlag, 2009.

[2] K. Zhou, J. C. Doyle, and K. Glover, Robust and Optimal Control. Prentice Hall, 1996.

[3] S. E. Mushi, Z. Lin, and P. E. Allaire, "Design, construction, and modeling of a flexible rotor active magnetic bearing test rig," *IEEE/ASME Transactions on Mechatronics*, vol. 17, no. 6, pp. 1170-1182, 2012.

[4] G. Li, Z. Lin, P. E. Allaire, and J. Luo, "Modeling of a high speed rotor test rig with active magnetic bearings," *ASME J. Vib. Acoust.*, vol. 128, no. 3, pp. 269-281, 2006.

[5] J. C. Doyle, K. Glover, P. P. Khargonekar and B. A. Francis, "State space solutions to standard H2 and H-infinity control problems," *IEEE Trans. Autom. Control.*, vol. 34, no. 8, pp. 831-847, 1989.

[6] S.E. Mushi, "Robust Control of Rotordynamic Instability in Rotating Machinery Supported by Active Magnetic Bearings," Ph.D. Dissertation, Uniersity of Virginia, Charlottesville, VA, 2012.